Nanoscale

Accepted Manuscript

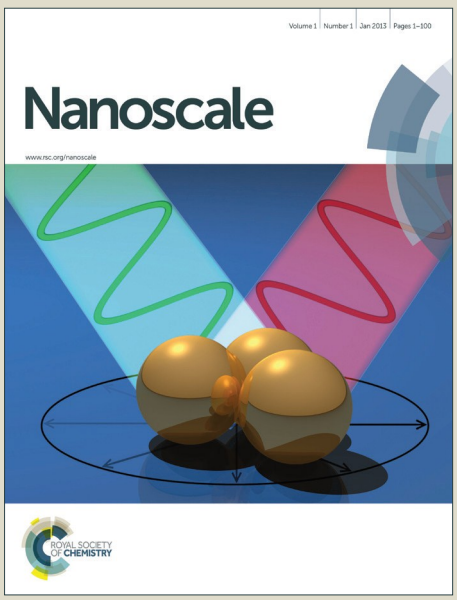

ROYAL SOCIETY OF CHEMISTRY

www.rsc.org/nanoscale

Journal Name

ARTICLE

Dynamics of nanocubes embedding into polymer films interrogated via spatially resolved plasmon modes

Adam Bottomley, Daniel Prezgot, Jason P. Coyle, and Anatoli Ianoul*

Received 00th January 20xx,
Accepted 00th January 20xx

DOI: 10.1039/x0xx00000x

www.rsc.org/

Integration of nanoparticles into thin films is essential for the development of functional materials, studies of fundamental interfacial processes, and exploitation of inherent properties from the particles themselves. In this work, we systematically investigate the process of incorporation of silver nanocubes into thin polystyrene films at temperatures just above the polymer glass transition. The process of nanocrystal incorporation can be precisely monitored via far-field spectroscopy to observe the response of spatially resolved hybrid plasmon modes. Each plasmon resonance has a distinct dynamic range and maximum sensitivity forming a complimentary set of nanorulers that operates over a distance comparable to the edge length of the cubes. The approach explored in this work is a general robust method for the development of long-range polychromatic nanorulers.

Introduction

The use of noble metal nanoparticles is extensive due to their ability to support localized surface plasmons yielding intense optical properties and extremely high sensitivities to material, geometry, and local environment.[1] Their optical properties are tunable across the ultraviolet to the infrared finding use in applications such as fluorescence enhancement,[2] surface-enhanced Raman spectroscopy,[3] catalysis,[4,5] sensing,[6] and photovoltaic enhancement.[7] They also lend themselves as effective nanorulers[8–11] for sub-diffraction measurements that can be performed using simple far-field observations while achieving spatial resolutions on the nanometer and in some cases angstrom scale.[12–14] The high sensitivity to changes in local environment surrounding plasmonic nanoparticles can be used to investigate phenomena such the glass transition of various polymer films allowing direct investigations into the thermodynamics of polymer interfaces.[15–22] These types of investigations are of importance as polymers are a common choice for solid supported nanomaterials.

Precise control over the relative orientation and distances of nanocrystals is critical in nanoscale engineering and design when the geometry of individual components in various nano-architectures defines their useful properties. In this respect, the ability to continuously monitor nanoscale assembly processes over large distances with high precision remains desirable yet challenging. To address these needs a wide variety of nanorulers utilizing various interactions and properties of plasmonic nanomaterials have been explored. This includes rulers based on coupling interactions between adjacent particles,[8,9,13,23,24] Fano interferences as a result of the interaction,[8,25] and particle coupling with metal surfaces.[12,14,26] Another common approach to plasmonic-based nanorulers utilizes the relationship between a plasmon and an emitter of some kind, including distance dependent surface enhanced Raman spectroscopy,[27] nanometal surface energy transfer interactions,[10,28,29] and plasmophore surface enhanced fluorescence.[30] The resolution, range, sensitivity, and ease of fabrication of nanorulers varies considerably, in some cases yielding angstrom resolution for interparticle/substrate coupling bands, while other systems can attain up to 100 nm in dynamic range such as the plasmophore based systems. A common element of the nanorulers described above is the interaction of a plasmonic particle with a specific nearby object, often this is another metal particle or surface, or an emitter such as a fluorophore or Raman label. Consequently, many of these systems need to be specifically calibrated for every circumstance as they are extremely sensitive to small changes in shape, orientation of the components, and local environment of the system itself. Alternatively some nanorulers are simply based on the change in refractive index of their surrounding environment. Refractive index sensing with inherent plasmonic modes does not need a coupling band or interaction with an emitter to function. These simple nanorulers have been shown to accurately determine the thickness of dielectric spacers up to 30 nm.[31]

Of particular interest, due to their ability to support strong hybridized modes,[32] silver nanocubes are an excellent candidate for use as a nanoruler and optical reporter in composite materials, as individual nanocubes are highly sensitive to anisotropy in their local envrionment.[33] Thus, it is possible to gain significant control over the optical properties of silver nanocubes, while also gaining insight into the position,

Department of Chemistry, Carleton University, 1125 Colonel By Dr. Ottawa, ON, Canada. E-mail: anatoli.ianoul@carleton.ca; Fax: +1 613-520-3749; Tel: +1 613-520-2600 ext 6043

† Electronic Supplementary Information (ESI) available: Topographical evolution of a nanocube monolayer visualized by AFM, a plot of relative signal change vs. time, and an experimental schematic depicting a system with a high refractive index sub-layer. See DOI: 10.1039/x0xx00000x

orientation, and degree of anisotropy in their local refractive index at any time. The spatially separated modes that occur when silver nanocubes are placed in an anisotropic environment allow for the resulting hybrid modes to be tuned independently for a small range in the visible spectrum. This level of control and information feedback about the conditions surrounding the nanocrystals makes this platform an effective tool for the production of composite materials with specific properties.

In the present work, we investigate how the sensitivities of hybrid plasmonic modes generated by anisotropy in the refractive index of the surrounding environment can yield significant control over the spectral signature of ensembles of silver nanocubes. In addition to spectral control the response of these hybrid modes to their changing environment allows them to be used as a set of three complementary nanorulers giving a combined dynamic range of ~60 nm. This is accomplished without the use of interparticle or substrate coupling bands or the use of emitters such as fluorophores or Raman labels.

Experimental

Chemicals

Silver nitrate ($AgNO_3$, 99%+), polyvinylpyrrolidone (PVP, M_w ~55 000), polystyrene (PS, M_w ~192 000), anhydrous 99.8% ethylene glycol (EG), sodium sulfide, toluene, and chloroform were purchased from Sigma-Aldrich and used as obtained. Ethanol (95%) was obtained from Commercial Alcohols and used without further purification. 1,2-dioleoyl-*sn*-glycero-3-phosphocholine (DOPC) was purchased from Avanti Polar Lipids as a powder and used as obtained.

Preparation of Nanocubes

Silver nanocubes were synthesized according to the procedure described in the literature.[34] To obtain larger cubes, 25 μL of 0.48 M sodium chloride in EG was added to the reaction flask prior to the injection of silver nitrate. When the characteristic peak found at ~350 nm was developed an additional 1.5 mL of 282 mM silver nitrate was added at a rate of 0.75 mL/min. The reaction was thermally quenched when the desired spectrum was observed.

Preparation of Polystyrene Thin Films

Polystyrene was dissolved in toluene to produce 1% and 0.5% w/w solutions which were then filtered through a 0.220 μm PTFE filter. Thin films were produced via static spin-coating on a Laurell WS-400-6NPP/LITE spin-coater. Films were allowed to anneal at 130 °C overnight.

Preparation of AgNC Monolayers

Nanocube substrates were prepared by forming Langmuir films on a NIMA 311D trough filled with Milli-Q water (18.2 MΩcm). An appropriate amount of AgNC and DOPC was dispersed in chloroform and deposited onto the surface of the water using a micro-syringe. Each monolayer was left for 20 min to allow complete chloroform evaporation. The surface pressure of the monolayer was measured with a paper Wilhelmy plate. Before transferring the monolayer onto solid supports several isotherm cycles were performed to anneal the films. Monolayers were transferred onto clean PS coated substrates at pressures corresponding to the gas phase of the isotherm via the Langmuir-Schaefer deposition method.

Heating of Supported Monolayers of PS Films

A small steel block connected to a thermocouple was placed on top of a hotplate and used to heat substrates placed on it for specific intervals. Substrates were periodic imaged via AFM and UV-Visible spectroscopy.

UV-Visible Measurements

Extinction spectra were obtained using a Cary 7000 equipped with a universal measurement analyzer. Spectra were processed and analyzed using OriginLab data analysis software.

Topographical Measurements

The topography of the NC monolayers transferred onto solid substrates was obtained using an Ntegra (NT-MDT, Russia) atomic force microscope in semi-contact mode in air at 21 °C with 512×512 or 1024×1024 points per image. A 100×100 μm^2 scanner (Ntegra) and cantilevers with rotated monolithic silicon tips (135 μm long, 0.3–6 N/m spring constant NSG03, resonance frequency 90 kHz, NT-MDT) were used for all topographic measurements. The typical scan rate was 0.5 Hz. AFM images were further processed by Nova image processing software.

Numerical Modelling

Finite difference time domain modelling was performed using Lumerical Solutions Inc. (FDTD Solutions v8.15). The simulation objects consisted of a 62 nm silver nanocube with a corner radius of 12.5 nm and a 2 nm capping layer of PVP supported by a 150 nm film of PS supported by an arbitrarily large SiO_2 substrate extended to the boundaries of the simulation (800 nm). The materials Ag,[35,36] PVP,[37] and PS,[38] were described by an analytical model fitted to tabulated permittivity data. A mesh override region extending at least 10 nm past the nanocube was used with a 0.5 nm mesh size. A total-field scattered-field (TFSF) light source was used, and perfect matched layer (PML) was used for the boundary conditions

Results and Discussion

Spectral Effects from Embedding Nanocubes into Polystyrene

Supported silver nanocubes show very characteristic extinction spectra that depend on the size of the cubes and the dielectric properties of the support.[39,40] There are two hybrid peaks

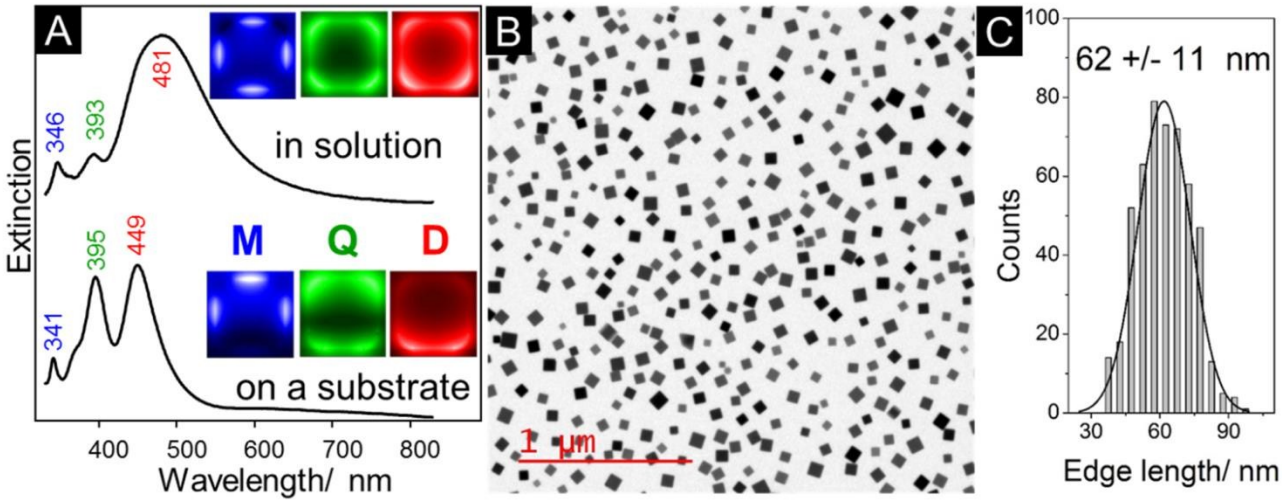

Fig. 1 (A) UV-visible extinction spectra of a nanocube sample in ethanol (top) and on a polystyrene substrate in air (bottom). E-field distributions for the dipolar (D), quadrupolar (Q), and multipolar (M) resonances are shown for both environments. (B) TEM image of as synthesized cubes. (C) Histogram showing size distribution in terms of edge length for the sample.

present in the spectra assigned as a dipolar and quadrupolar surface plasmon resonances. These hybrid modes are at their sharpest when the cube is not coupling to another metal surface. Plasmonic coupling produces a peak at a longer wavelength, while also making the inherent peaks more broad and less distinguished.[41,42]

In this work nanocubes with the average edge length 62 ± 11 nm (Figure 1), were studied. The size distribution is not particularly narrow, however the size dependence for the position of the quadrupolar resonance is relatively weak[43] and the corresponding UV-vis extinction spectrum shows characteristic sharp signatures with relatively narrow half widths when on a substrate. The dipole (D) resonance for the nanocubes while in solution is at 481 nm with the measured full width at half maximum (FWHM) around 90 nm (Figure 1A). Other higher order resonances present in the solution spectrum are at 393 and 346 nm. The E-field distribution corresponding to these modes is shown as insets in Figure 1A and appears to be symmetrical.

When supported by a thin polystyrene (PS) film the cubes exhibit narrow hybrid dipolar resonance[32] (D) at 449 nm (FWHM ~40 nm), a hybrid quadrupolar resonance (Q) at 395 nm (FWHM 30 nm), and a multipolar resonance (M) at 341 nm (14 nm) (Figure 1A). Assignment and spatial distribution of the resonances have been studied theoretically and experimentally, for example using electron energy loss spectroscopy[44–47] and cathodoluminescence.[48] The E-field distribution maps (Figure 1A inset) show that the E-field associated with the hybrid dipolar resonance is primarily located at the bottom part of the cube, quadrupolar at the top, and multipolar resonances have their significant component associated with the sides of the cube. This spatially resolved nature of plasmonic modes as well as small FWHMs enables us to precisely monitor the dynamics and changing local environment around the nanocubes as they embed into their supporting polymer.

At room temperature PS exists in the glassy state and can therefore act as a dielectric substrate smooth enough to support nanocube monolayers. Bulk PS experiences a glass transition at ~ 100 °C.[49] While the transition temperature depends on factors such as the chain length and tacticity, a significant depression in the T_g to ~ 75 °C occurs for ultra-thin films.[50] Extinction spectra of the nanocube monolayers are allowed to evolve over time when the system is kept above the supporting PS glass transition temperature at 112 ± 1 °C (Figure 2). The observed changes do not result from nanocube transformation, such as rounding or oxidation,[43] but from their response to being embedded into the PS film. Exclusion of thermally induced damage was addressed by comparing the PS supported sample to a glass supported sample. The glass supported cubes, heated alongside the PS supported cubes showed no changes in their extinction spectrum at the end of the experiment. Therefore, the observed spectroscopic evolution is associated with the nanocrystals embedding into the polystyrene film exclusively.

The spectroscopic changes that occur with time can be separated into four stages shown in Figure 2. The first stage is characterized by a very strong red-shift of the D resonance from the original 449 nm to 480 nm. Both the position and intensity of the Q resonance remain almost invariant. In the M resonance region, a peak around 350 nm is developed in addition to the original peak at 341 nm.

During the second stage both D and Q resonances slightly red-shift. At the same time, the M resonance shows a two state-like transition between the peaks at ~ 341 nm and ~ 350 nm. During the third stage, the D resonance reaches a max at 485 nm, Q shows the greatest redshift to ~ 414 nm, the resonance at 340 disappears, leaving only a 350 nm multipolar resonance in the region. Finally, during the fourth stage the D and M resonances remain unchanged. At the same time, the Q resonance becomes obscured by the overlap with the D mode.

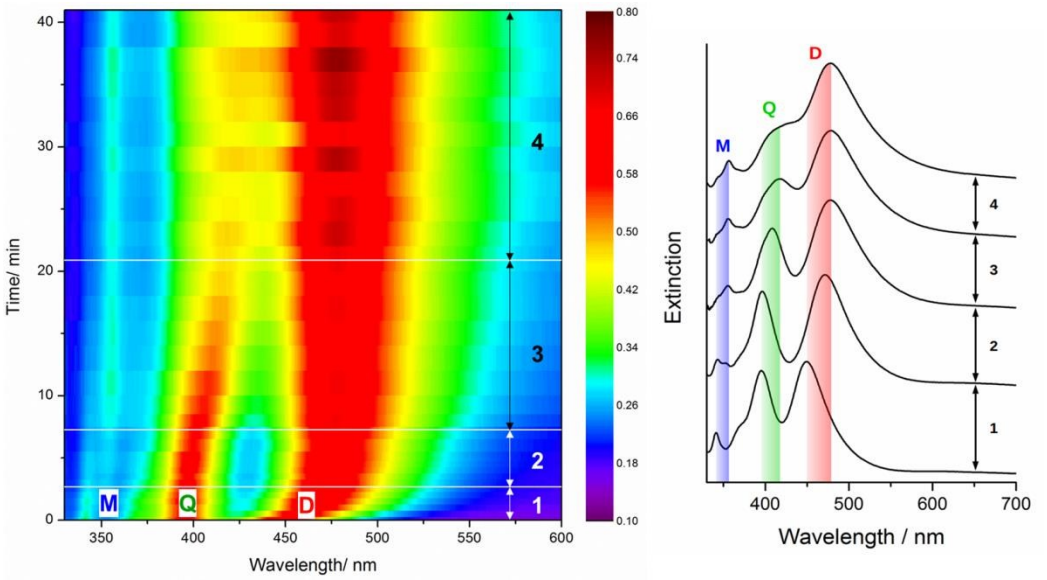

Fig. 2 (Left) Contour plot depicting the attenuation of light as a function of time. Contributions from plasmon modes are labelled as dipolar (D), quadrupolar (Q), and multipolar (M). (Right) Single extinction spectra corresponding to the horizontal lines on the contour plot. The red, green, and blue bands indicate the overall shift for D, Q, and M modes respectively

The spectral changes can be reasonably well explained by the process of incorporation of nanocubes into the PS film upon heating as observed by AFM (Figures 3 and S1). As a result of incorporation, the environment surrounding the nanocubes becomes more isotropic and the spectrum moves towards that of nanocubes in a high refractive index solution as hybridization of the plasmonic modes is reduced.

Extinction Spectrum as Nanoruler

Detailed AFM measurements of the nanocube monolayer for each stage of spectroscopic changes help to better determine the relationship between the geometry of the system and its optical signature. According to AFM measurements, the average height of the nanocube monolayer decreases with heating time (Figure S1). The original untreated monolayer showed an average height of 75 nm above the substrate (Figure 3A, S1). This is somewhat greater than the average size of the nanocubes as determined form TEM (Figure 1, 62 nm). The discrepancy can be accounted for by the PVP layer around the nanocube, which can be 1-4 nm in thickness[51] and imperfections of the topographic analysis. Upon further heating for 15 min the average height of the monolayer decreases to ~ 50% of the nanocubes edge length. After 40 min of heating the average height of the cubes within the monolayer is only around 8 nm.

It is possible to correlate the spectral changes in the NC/PS system to the average exposed height of the nanocrystals. For example, in this particular experiment (under specific heating conditions and geometry) the four stages described above and exemplified by Figures 2, 3 and S1, correspond to the following changes in the AFM data:

1. During the first stage (less than 2 minutes of heating) the average height of the nanocubes within the monolayer decreases from 75 nm to 55 nm while retaining their orientation and spatial arrangement. This region has the highest overall sensitivity and is dominated by the peak shift of the dipolar resonance.

2. During the second stage the average height of the exposed nanocubes decreases to ~ 45 nm, occurring between 2 and 7 minutes of heating. The most sensitive observable for this stage is the emergence of a pair of multipolar (M) modes at ~ 341 and 350 nm. As the particles embed further into the substrate the full transition of peak intensity from the higher energy to the lower energy M mode occurs. Additionally a portion of the cube population begins to experience a tilting motion during this stage.

3. The third stage, (7 – 21 minutes) sees further incorporation of the cubes into the polymer layer. The average height decreases below 30 nm, which is roughly half of the nanocube size. By this point nearly all of the cubes have experienced some type of tilting motion. During this stage, the sensitivity of the Q mode is at its greatest.

4. The final stage in this experiment corresponds to almost complete submergence of the particles. The average height decreases to less than 25 nm with the majority of cubes having only a single corner exposed. This stage has the least sensitivity of the four and is associated with a loss of anisotropy in the local environment around the cubes.

This analysis clearly indicates that with the help of three independent and spatially separated spectroscopic markers D, Q, and M it is possible to monitor the position of embedded nanoparticles over the distance of ~ 60 nm. The maximum sensitivity for each of the markers occurs at 0, 22, and 36 nm of depth for D, M, and Q modes respectively and therefore provides an opportunity to measure not only very short distances, but also short lateral displacement over an extended range greater than any of the modes individually.

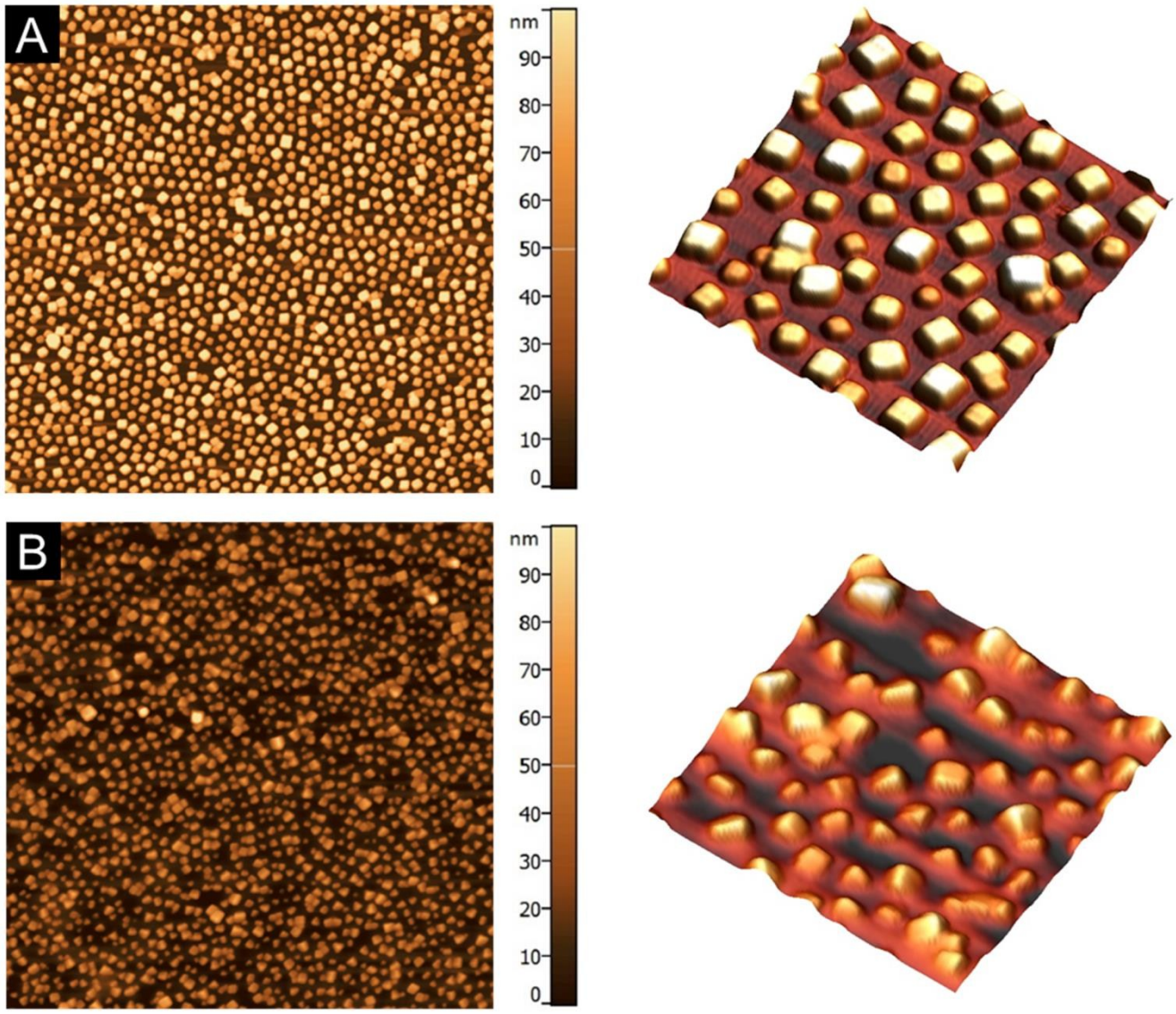

Fig. 3 AFM images (5×5 μm² left, and 1×1 μm², right) of nanocube monolayers (A) initially and (B) after heating for 30 min at 112 °C.

For a nanocube on top of the PS film (embedding depth 0 nm) the E-field is distributed around the bottom, middle and top of the supported cube observed for the D, M, and Q resonances respectively (Figure 1A). As the nanocube embeds into the polymer the three resonances sense changes in the environment during different time intervals (Figure S2). The dependencies can be fairly well fitted with mono-exponential decaying function shown in equation (1)

$$Relative\ signal\ increase = I_0 - I_1 e^{\frac{-(t-t_0)}{\tau}} \quad (1)$$

where I_0, I_1, and t_0 are fitting parameters to give characteristic time constants τ of 1.6, 9.3, and 23.4 minutes for D, M, and Q responses respectively.

As the rate of incorporation of the nanocrystals into the polymer film is a function of temperature and the glass transition temperature of a thin polymer film is dependent on many factors such as film thickness,[50] we plot the relative spectral features as a function of depth of immersion of the cubes into the film to yield relationship that is dependent only on the position of the cubes. Figure 4 shows the normalized relative response of peak positions for the D and Q modes, and the relative intensity of the M modes. Dipolar and quadrupolar relationships can be expressed as peak shift in nanometers over distance in nanometers yielding sensitivities in units of nm / nm (spectral / physical). The dipolar resonance shows the greatest sensitivity at the initial point of the experiment of 2.1 nm / nm decreasing exponentially as the cubes become further imbedded into the polymer. Initially, the Q mode is insensitive to the changing environment around the cube, but rapidly increases in sensitivity after ~ 20 nm of immersion to a maximum of 1.2 nm/nm at 36 nm depth, roughly half the edge length of the cubes. The transition between the M resonances is not one of spectral shift, but the disappearance of one mode and the emergence of the other and thus the sensitivity is the percentage change in nm^{-1} and is strongly dependent on the sensitivity of the instrumentation used for measurement. This transition has a dynamic range between 10 and 35 nm of

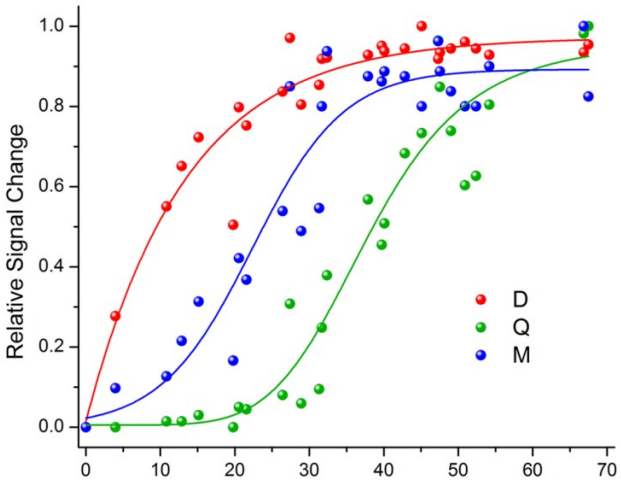

Fig. 4 Evolution of plasmonic modes as a function of nanocrystal depth. Red and green data points correspond to the normalized peak shift versus particle depth for the dipolar (D) and quadrupolar (Q) modes respectively. The blue data points represent the relative change in intensities of the multimode (M) resonances versus depth of nanocube immersion. Fitted lines are empirical and based on a mono-exponential decay for D, and logistic functions for Q and M modes.

embedding with a maximum sensitivity of found at 22 nm. This maximum corresponds to the condition when both multipolar resonances are present and of equal intensity and conveniently supplements the low point in observed sensitivity at the intersection of the D and Q modes.

Free Energy Change on Embedding a Particle

The driving force for incorporation of nanocubes into a PS film is described by the Helmholtz free energy decrease A_s as determined by Kovacs *et al.*[15,16,22] If we assume initial and final states are $A_s = a\gamma_1$ and $A_s = a\gamma_{12}$ where a is area, and γ_1 and γ_{12} are the surface energies of a non-interacting nanocrystal surface and the interface between the nanocrystal and the substrate, the change in surface free energy is described by equation (2) such that if $\gamma_1 > \gamma_{12}$ then $\Delta A_s < 0$ and the interaction is spontaneous.

$$\Delta A_s = a(\gamma_{12} - \gamma_1) \quad (2)$$

Satisfying equation 2 is sufficient to determine if particles will begin incorporating themselves into the polymer, but it is insufficient to predict if particles will become fully embedded. If the system reaches a local minimum at any point before particles become fully embedded the sinking process will cease.[15] If we consider the reformation of the polystyrene surface with energy γ_2 as the particle continues to sink it becomes apparent that to remain spontaneous the surface energy of the particle must be greater than the sum of the interfacial surface energy and the polymer surface energy yielding inequality (3).

$$\gamma_1 > \gamma_2 + \gamma_{12} \quad (3)$$

During this experiment we did not observe the full immersion of nanocubes into polystyrene, even at extended times in excess of 1 hour and elevated temperatures up to 140 °C. As such, this system fails to satisfy inequality (3) and suggests that we observed the intermediate regime that is described by inequality (4).

$$\gamma_{12} < \gamma_1 < \gamma_2 + \gamma_{12} \quad (4)$$

This equation states that the surface tension of the underlying polymer is simply too high relative to the particle surface energy to allow the particles to fully embed themselves. This conclusion is consistent with experimental observations by other groups that have succeeded in fully embedding silver nanocubes into polystyrene only by solvent annealing under vacuum,[52] which effectively lowers the surface tension of the polymer satisfying inequality (3). Additionally, observing this regime is a direct consequence of utilizing surface passivated nanocrystals. The surface energy of bulk polyvinylpyrrolidone[53] and polystyrene[54] are similar at ~43 and 33 mJ/m^2 respectively and significantly lower than that of bare metals. For example, Kovacs et al,[15] lists the surface energy for bare silver at 1100 mJ/m^2 which is two orders of magnitude above the surface energy of polystyrene effectively forcing inequality (3) to always be true for an unpassivated silver particle. The mechanism for fully embedding particles is often reported with the generation of wetting layer around 1 nm thick.[17,18] This does not occur in our experiment as this would satisfy inequality (3) and lead to fully embedded particles. This relationship sheds some light on the surface energy of the interface between the particle and the polymer, but also opens experimental avenues to produce nanocomposites that allow for control over physical access to the surface of the nanocrystals.

Spectra of Partially Embedded Cubes: Modelling

To investigate the process in more detail the finite-domain time-difference (FDTD) method was used to model the extinction spectra of a nanocube embedded iteratively in 5 nm steps into a polystyrene film (Figure 5). The nanocube's orientation as well as the light source's angle of incidence were kept normal to the substrate. As the nanocube is lowered into the substrate a rapid shift in the D mode is initially observed while the Q remains relatively insensitive; the D mode shifts ~ 60 nm while the Q only shifts ~ 5 nm at 30 nm of immersion. As the cube is further immersed in the substrate the sensitivity of the D mode gradually diminishes as the Q mode's sensitivity increases until it reaches a maximum at 55 nm of immersion. This results in a red-shift of the Q mode by ~ 50 nm between 30 nm and 60 nm of immersion, while the D mode only shifts 15 nm (Figure 5)

In general this model reliably follows the trends observed experimentally. When comparing sensitivities derived from the simulations to experimentally observed values we find the D mode is shown to have a maximum sensitivity of 4.0 nm / nm as opposed to 2.1 nm / nm while the Q reaches a maximum of 1.8 nm / nm as opposed to 1.2 nm / nm. The increased sensitivity is

a consequence of the model describing an idealized scenario involving only a single nanocube. The experimental measurements are performed on an ensemble of nanocubes which introduce a degree of polydispersity in terms of size, depth of immersion, and orientation, all of which contribute to band-broadening and consequently a reduction in the sensitivity when compared to the single particle model.

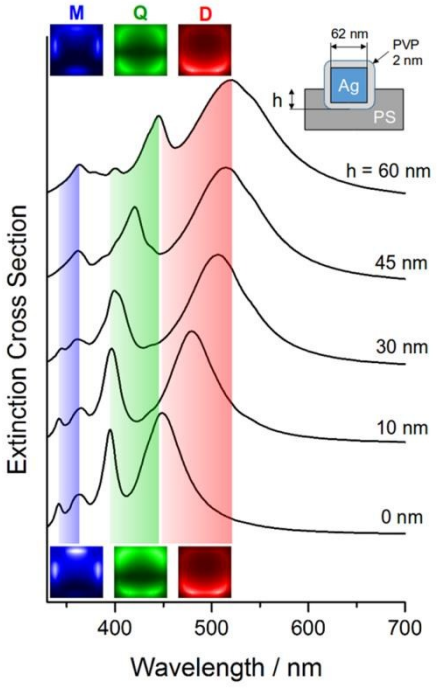

Fig. 5 FDTD calculated extinction spectra of a silver nanocube in polystyrene film for different embedding depths. E-Field distributions (imbedded) are given for the initial and final states of the simulation. The red, green, and blue bands indicate the overall shift for D, Q, and M modes respectively

While a general agreement between the model and experimental results was obtained, it should be noted that the model begins to diverge from the experimental results after the cube is immersed at a depth greater than half its edge length. While almost no further peak shift of the D mode was observed after the cubes are half immersed experimentally (Figure 4), the model predicts a further peak shift of 20 nm during the second half of the experiment (Figure 6A). The Q mode also shifts relatively faster experimentally than predicted by the model; the predicted point of maximum sensitivity of the Q mode is after the nanocubes have been immersed 55 nm, while we observe this point at 36 nm of immersion in the experiment. A shift to lower energy for the M mode is predicted by the model occurring after the cube has been half-immersed, while the actual transition observed experimentally occurs at a much earlier stage. Error tends to be significant in modelling the imaginary component of the dielectric function in this region of the spectrum for silver. The discrepancy is attributed to interference from the interband transition edge for silver ~3.8 eV (326 nm) affecting a small spectral range near this position.[36] For this reason we do not discuss the modelled results of the M mode in detail. The divergence between the model and experimental results primarily corresponds with our third stage of experimental observations where tilting of the nanocubes

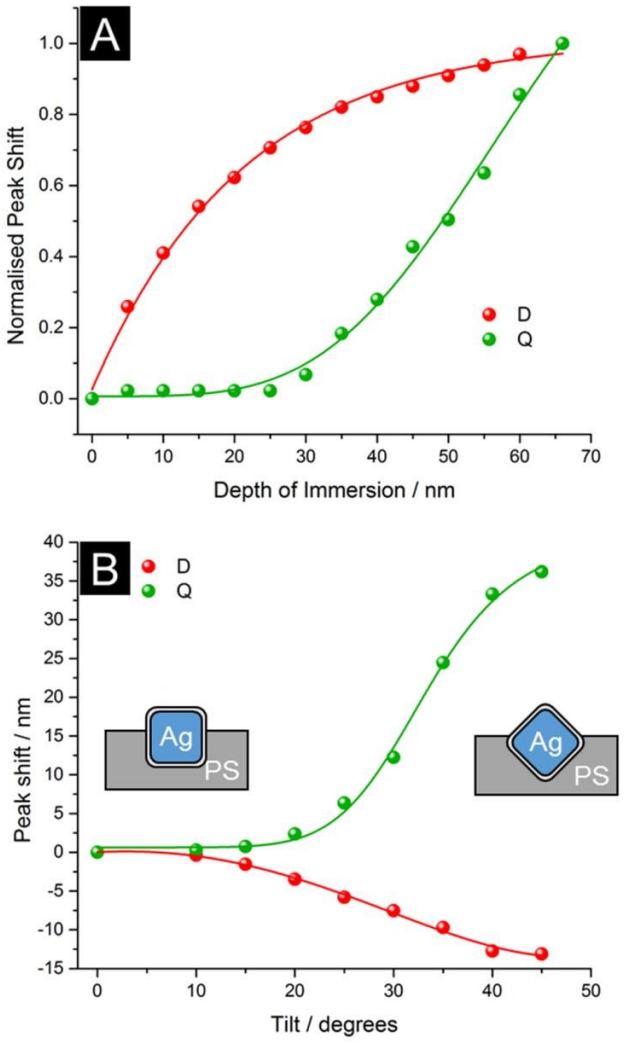

Fig 6 Peak shifts from FDTD modelling displaying: (A) Normalized peak shift versus depth of immersion for a normal oriented 62 nm cube imbedding into polystyrene. (B) Relative peak shift against angle of tilt about a single axis for a 62 nm cube held at a constant depth of 40 nm in polystyrene. Very little change is observed at a small angles (< 15°), but increasing the angle of tilt results in a small blue shift of the D mode and a rapid red shift of the Q mode.

becomes significant. The model described thus far has consisted of a nanocube orientated normal to the substrate. It therefore becomes necessary to examine the effect of nanocube orientation on the optical properties of the particle in order to consolidate the predicted and experimental results.

Effects of Nanocube Orientation on Extinction Spectra

FDTD simulations were utilized to independently examine the effect of nanocube orientation on their extinction spectra using an unpolarized light source orientated perpendicular to the substrate, which we define as the z axis. A series of simulations was performed on cube immersed 40 nm into polystyrene, which was rotated between 0° and 45° about a single axis through its center. Experimentally the cubes are free to rotate along three degrees of freedom in terms of x, y and z axes.

Individual rotation about the x and y axes are degenerate in terms of spectral response while rotation about the z axis is unobservable as all orientations are present at the initial and final states of the experiment. We observe cubes having rotated about both x and y axes at a variety of angles after 30 minutes of heating (Figure 3), with the majority having rotated to large angles (> 25°) on at least one of the two axes. Figure 6B describes the peak shift of the D and Q modes as the cube is rotated about a single axis. A rotation of less than 15° results in very little spectral response, but further rotation results in a blue shift of the D mode by 13 nm and a red shift of the Q mode up to 36 nm at 45°. By contrasting these spectral shifts against those associated with the normal-oriented cube model we illustrate that the experimental shifts in the final stages of the experiment arise from the combination of the nanocube immersion and change in orientation which occur simultaneously. While a small (~15 nm) red shift of the D mode is predicted for the last 20 nm of immersion of a normal-oriented nanocube (Figure 6A), the change in orientation of the nanocube results in a comparable blue shift. The competition between these phenomena leads to the observation of the apparent saturation of the shift of the D mode. Meanwhile, the red shift of the Q mode associated with the change in orientation of the nanocube accumulates with the red shift associated with further immersion of the nanocube. The combined effect leads to a more rapid shift the Q mode than would be observed if the nanocube did not change orientation.

Subfacial Sensitivity of Hybridized Modes

As long as there is refractive index contrast present in a system spatially resolved plasmon modes can be used to track the changes in their surroundings. The initial optical signature and spectral evolution of the system as particles embed themselves into the polymer layer are dependent on the refractive index of the surrounding environment above the system, the polymer itself, and in cases where the particle can migrate near the bottom of the polymer film the refractive index of the underlying solid support will have a significant impact on the spectral features of the film. As the system evolves, it moves from a strongly hybridized regime resulting from high anisotropy to a more isotropic system that results in less hybridization as the cubes embed themselves into the polymer layer. However, if a the polymer layer is chosen such that it is thin enough that cubes can nearly reach the bottom of it, and the film is situated on a substrate of relatively high refractive index it becomes possible to push the system back in the direction of hybridization by inducing anisotropy within the material. This scenario was experimentally explored by using a thin polystyrene film (~ 50 nm) on top of a high refractive index substrate of titanium oxide (Figure S3). As a result of the increased refractive index of the substrate, the D mode does not saturate before the cubes stop embedding. As the relative refractive indices of both the substrate and superstrate are higher than the initial setup at time zero, all modes are red shifted but maintain a degree of hybridization. This system adds an extra dimension to the nanoruler, extending its dynamic range. Similar improvements can be made by choosing a higher refractive index polymer, again increasing the sensitivity and dynamic range of the system. High-n polymers such as polyphosphazenes and polyphosphonates provide an attractive alternative to polystyrene due to their high refractive index, up to 1.75 compared to polystyrene's n of 1.60 at 550 nm as well as a similar T_g and processability.[55] FDTD modelling was employed to compare the refractive index sensitivity of the nanoruler on a polymer with n = 1.75 against the polystyrene model. An improvement in the maximum sensitivity of both the D and Q mode was observed. The D mode's initial sensitivity increases from 4.0 to 5.0 nm / nm, while the Q mode's maximum sensitivity increases from 1.8 to 2.2 nm / nm at 50 nm of immersion. With alternative material choices of both the substrate and polymer film; provided the process of incorporation remains energetically favourable, it becomes possible to further improve the sensitivity and dynamic range for this type of nanoruler.

Conclusions

We fabricated a nanocomposite comprised of silver nanocube monolayers on polystyrene thin films as a platform for the precise control and observation of nanoparticles embedding into a polymer. This platform is a useful avenue for the investigation of surface energies and interfacial energies between surface passivated nanocrystals and polymer matrices yielding insight into the behaviour and driving forces acting on the particles. We have also determined that once a system is carefully calibrated it becomes possible to know the average distance and orientation of the nanocrystals embedded into the polymer using simple far field optical measurements alone. This type of anisotropic nanoruler is based on plasmon hybridization induced by proximity to a dielectric substrate and utilizes the combined refractive index sensitivity of the spatially resolved plasmon modes. Contrary to a system based on interparticle and substrate-particle coupling modes, or particle-emitter combinations, the use of hybrid modes to determine the anisotropy of the local environment is a simple platform utilizing inherent properties of the particles while yielding a reasonably large quasilinear dynamic range similar to the size of the particle itself. The platform described above is a general robust approach to nano-positioning and sensing, and can be easily modified to include additional parameters such as a high refractive index substrate below the polymer-nanocrystal composite.

Acknowledgements

Financial support was provided by NSERC.

References

1 C. Noguez, *J. Phys. Chem. C*, 2007, **111**, 3806–3819.
2 A. Ianoul and A. Bergeron, *Langmuir*, 2006, **22**, 10217–10222.
3 P. C. Lee and D. Meisel, *J. Phys. Chem.*, 1982, **86**, 3391–3395.

4 H. Robatjazi, S. M. Bahauddin, C. Doiron and I. Thomann, *Nano Lett*., 2015, **15**, 6155–6161.
5 J. R. Adleman, D. A. Boyd, D. G. Goodwin and D. Psaltis, *Nano Lett*., 2009, **9**, 4417–4423.
6 A. D. McFarland and R. P. Van Duyne, *Nano Lett*., 2003, **3**, 1057–1062.
7 H. Tan, R. Santbergen, A. H. M. Smets and M. Zeman, *Nano Lett*., 2012, **12**, 4070–4076.
8 J. Butet and O. J. F. Martin, *ACS Nano*, 2014, **8**, 4931–4939.
9 S. Shen, L.-Y. Meng, Y. Zhang, J. Han, Z. Ma, S. Hu, Y. He, J.-F. Li, B. Ren, T.-M. Shih, Z. Wang, Z.-L. Yang and Z.-Q. Tian, *Nano Lett*., 2015, **15**, 6716–6721.
10 R. E. Armstrong, R. A. Riskowski and G. F. Strouse, *Photochem. Photobiol*., 2015, **91**, 732–738.
11 X. Wang, S. Li, P. Zhang, F. Lv, L. Liu, L. Li and S. Wang, *Adv. Mater*., 2015, **27**, 6040–6045.
12 R. T. Hill, K. M. Kozek, A. Hucknall, D. R. Smith and A. Chilkoti, *ACS Photonics,* 2014, **1**, 974–984.
13 B. Gallinet, T. Siegfried, H. Sigg, P. Nordlander and O. J. F. Martin, *Nano Lett*., 2013, **13**, 497–503.
14 R. T. Hill, J. J. Mock, A. Hucknall, S. D. Wolter, N. M. Jokerst, D. R. Smith and A. Chilkoti, *ACS Nano*, 2012, **6**, 9237–9246.
15 G. . Kovacs and P. . Vincett, *J. Colloid Interface Sci*., 1982, **90**, 335–351.
16 G. J. Kovacs and P. S. Vincett, *Thin Solid Films,* 1984, **111**, 65–81.
17 R. D. Deshmukh and R. J. Composto, *Langmuir*, 2007, **23**, 13169–13173.
18 J. Erichsen, J. Kanzow, U. Schürmann, K. Dolgner, K. Günther-Schade, T. Strunskus, V. Zaporojtchenko and F. Faupel, *Macromolecules*, 2004, **37**, 1831–1838.
19 S. a. Hutcheson and G. B. McKenna, *Phys. Rev. Lett.*, 2005, **94**, 076103.
20 J. Teichroeb and J. Forrest, *Phys. Rev. Lett*., 2003, **91**, 016104.
21 J. S. Sharp, J. H. Teichroeb and J. A. Forrest, *Eur. Phys. J. E*, 2004, **15**, 473–487.
22 G. J. Kovacs, J. *Vac. Sci. Technol*., 1982, **20**, 419.
23 P. K. Jain, W. Huang and M. A. El-Sayed, *Nano Lett*., 2007, **7**, 2080–2088.
24 A. I. Dolinnyi, *J. Phys. Chem. C*, 2015, **119**, 4990–5001.
25 N. Liu, M. Hentschel, T. Weiss, A. P. Alivisatos and H. Giessen, *Science*, 2011, **332**, 1407–1410.
26 A. Moreau, C. Ciracì, J. J. Mock, R. T. Hill, Q. Wang, B. J. Wiley, A. Chilkoti and D. R. Smith, *Nature*, 2012, **492**, 86–89.
27 A. K. Singh, S. A. Khan, Z. Fan, T. Demeritte, D. Senapati, R. Kanchanapally and P. C. Ray, *J. Am. Chem. Soc*., 2012, **134**, 8662–8669.
28 C. J. Breshike, R. A. Riskowski and G. F. Strouse, *J. Phys. Chem. C*, 2013, **117**, 23942–23949.
29 X. Zhang, C. a. Marocico, M. Lunz, V. a. Gerard, Y. K. Gun'ko, V. Lesnyak, N. Gaponik, A. S. Susha, A. L. Rogach and a. L. Bradley, *ACS Nano*, 2012, **6**, 9283–9290.
30 G. R. Bourret, T. Ozel, M. Blaber, C. M. Shade, G. C. Schatz and C. A. Mirkin, *Nano Lett*., 2013, **13**, 2270–2275.
31 L. Li, T. Hutter, W. Li and S. Mahajan, *J. Phys. Chem. Lett*., 2015, **6**, 2282–2286.
32 S. Zhang, K. Bao, N. J. Halas, H. Xu and P. Nordlander, *Nano Lett*., 2011, **11**, 1657–1663.
33 N. Ahamad, A. Bottomley and A. Ianoul*, J. Phys. Chem. C*, 2012, **116**, 185–192.
34 S. E. Skrabalak, L. Au, X. Li and Y. Xia, *Nat. Protoc*., 2007, **2**, 2182–2190.
35 E. D. Palik, Handbook of Optical Constants, Academic Press, San Diego, 1998.
36 H. U. Yang, J. D'Archangel, M. L. Sundheimer, E. Tucker, G. D. Boreman and M. B. Raschke, *Phys. Rev. B*, 2015, **91**, 235137.
37 T. A. F. König, P. A. Ledin, J. Kerszulis, M. A. Mahmoud, M. A. El-Sayed, J. R. Reynolds and V. V Tsukruk, *ACS Nano*, 2014, **8**, 6182–92.
38 N. Sultanova, S. Kasarova and I. Nikolov, *Acta Phys. Pol. A*, 2009, **116**, 585–587.
39 L. J. Sherry, S.-H. Chang, G. C. Schatz and R. P. Van Duyne, *Nano Lett*., 2005, **5**, 2034–2038.
40 Q. Zhang, W. Li, C. Moran, J. Zeng, J. Chen, L. P. Wen and Y. Xia, *J. Am. Chem. Soc*., 2010, **132**, 11372–11378.
41 N. Ahamad and A. Ianoul, *J. Phys. Chem. C*, 2011, **115**, 3587–3594.
42 M. Mahmoud, C. Tabor and M. El-Sayed, *J. Phys. Chem. C*, 2009, **113**, 5493–5501.
43 E. Ringe, J. M. McMahon, K. Sohn, C. Cobley, Y. Xia, J. Huang, G. C. Schatz, L. D. Marks and R. P. Van Duyne, *J. Phys. Chem. C*, 2010, **114**, 12511–12516.
44 O. Nicoletti, F. de la Peña, R. K. Leary, D. J. Holland, C. Ducati and P. A. Midgley, *Nature*, 2013, **502**, 80–84.
45 M. Bosman, V. J. Keast, M. Watanabe, A. I. Maaroof and M. B. Cortie, *Nanotechnology*, 2007, **18**, 165505.
46 S. Mazzucco, N. Geuquet, J. Ye, O. Stéphan, W. Van Roy, P. Van Dorpe, L. Henrard and M. Kociak, *Nano Lett*., 2012, **12**, 1288–1294.
47 D. Rossouw, M. Couillard, J. Vickery, E. Kumacheva and G. A. Botton, *Nano Lett*., 2011, **11**, 1499–1504.
48 E. J. R. Vesseur, R. de Waele, M. Kuttge and A. Polman, *Nano Lett*., 2007, **7**, 2843–2846.
49 J. Rieger, *J. Therm. Anal*., 1996, **46**, 965–972.
50 G. Vignaud, M. S. Chebil, J. K. Bal, N. Delorme, T. Beuvier, Y. Grohens and A. Gibaud, *Langmuir*, 2014, **30**, 11599–11608.
51 A. Kyrychenko, O. M. Korsun, I. I. Gubin, S. M. Kovalenko and O. N. Kalugin, *J. Phys. Chem. C,* 2015, **119**, 7888–7899.
52 B. Gao, G. Arya and A. R. Tao, *Nat. Nanotechnol*., 2012, **7**, 433–437.
53 J. Brandrup, E. H. Immergut and E. A. Grulke, Polymer Handbook, New York: Wiley, 4th edn., 1999.
54 M. K. Chaudhury, *Mater. Sci. Eng. R Reports*, 1996, **16**, 97–159.
55 T. Higashihara and M. Ueda, *Macromolecules*, 2015, **48**, 1915–1929.